







Asymmetries in the Simulated Ozone Distribution on TRAPPIST-1e due to Orography

Anand Bhongade¹ , Daniel R Marsh^{2,3} , Felix Sainsbury-Martinez² , and Gregory Cooke^{2,4} ¹ School of Earth and Environment, University of Leeds, Leeds, LS2 9JT, UK² School of Physics and Astronomy, University of Leeds, Leeds, LS2 9JT, UK³ School of Chemistry, University of Leeds, Leeds, LS2 9JT, UK⁴ Institute of Astronomy, University of Cambridge, Cambridge, CB3 0HA, UK

Received 2024 July 3; revised 2024 October 6; accepted 2024 November 4; published 2024 December 5

Abstract

TRAPPIST-1e is a tidally locked rocky exoplanet orbiting the habitable zone of an M dwarf star. Upcoming observations are expected to reveal new rocky exoplanets and their atmospheres around M dwarf stars. To interpret these future observations we need to model the atmospheres of such exoplanets. We configured Community Earth System Model version 2–Whole Atmosphere Community Climate Model version 6, a chemistry climate model, for the orbit and stellar irradiance of TRAPPIST-1e assuming an initial Earth-like atmospheric composition. Our aim is to characterize the possible ozone (O₃) distribution and explore how this is influenced by the atmospheric circulation shaped by orography, using the Helmholtz wind decomposition and meridional mass streamfunction. The model included Earth-like orography, and the substellar point was located over the Pacific Ocean. For such a scenario, our analysis reveals a north–south asymmetry in the simulated O₃ distribution. The O₃ concentration is highest at pressures >10 hPa (below ~30 km) near the south pole. This asymmetry arises from the higher landmass fraction in the northern hemisphere, which causes drag in near-surface flows and leads to an asymmetric meridional overturning circulation. Catalytic species were roughly symmetrically distributed and were not found to be primary driver for the O₃ asymmetry. The total O₃ column density was higher for TRAPPIST-1e compared to Earth, with 8000 Dobson units (DUs) near the south pole and 2000 DU near the north pole. The results emphasize the sensitivity of O₃ to model parameters, illustrating how incorporating Earth-like orography can affect atmospheric dynamics and O₃ distribution. This link between surface features and atmospheric dynamics underlines the importance of how changing model parameters used to study exoplanet atmospheres can influence the interpretation of observations.

Unified Astronomy Thesaurus concepts: [Exoplanet atmospheres \(487\)](#); [Exoplanet atmospheric composition \(2021\)](#); [Exoplanet atmospheric dynamics \(2307\)](#); [Transmission spectroscopy \(2133\)](#); [James Webb Space Telescope \(2291\)](#)

1. Introduction

Scientists have long wondered about the existence of life on other planets, and this curiosity has motivated them to explore celestial bodies beyond our solar system. To date, over 5600 confirmed exoplanets have been identified by instruments like the Kepler Space Telescope, the Transiting Exoplanet Survey Satellite, and various space-based and ground-based telescopes.⁵ Studies utilizing Kepler mission data have found that the presence of small rocky exoplanets around M dwarf stars exceeds that around Sun-like stars (A. W. Howard et al. 2012; C. D. Dressing & D. Charbonneau 2015; G. D. Mulders et al. 2015; E. Gaidos et al. 2016), although this is likely because of the observational bias of telescopes for detecting exoplanets around smaller, cooler, and dimmer stars. To date, 200 confirmed rocky exoplanets have been detected.⁶

M dwarf stars, constituting approximately 70% of all known stars in our galaxy, have garnered scientific attention due to their abundance and compact planetary systems (J. J. Bochanski et al. 2010). The location of the habitable zone around a star

depends upon its stellar properties (S.-S. Huang 1959). M dwarf stars, characterized by their low temperature and flux, have habitable zones situated closer to them. Detection methods such as transit photometry and radial velocity rely on the planet-to-star mass and size ratio, making the search for rocky exoplanets in habitable zones around M dwarf stars more feasible due to the star's relatively small size (A. Gould et al. 2003; P. Nutzman & D. Charbonneau 2008; A. L. Shields et al. 2016; A. Reiners et al. 2018).

Exoplanets orbiting M dwarfs can be in such proximity to their stars that they become tidally locked, resulting in a permanent dayside and nightside. Tidal locking occurs due to the gravitational force exerted by the star, which distorts the planet into an elongated shape. This results in synchronous rotation, where the planet's rotational period equals its orbital period (R. Barnes 2017).

In addition to the incident energy flux from the host star and orbital configuration, a planet's location relative to the habitable zone is significantly influenced by atmospheric composition, particularly the presence or absence of greenhouse gases. Ozone (O₃), acting as a greenhouse gas on Earth, influences the vertical temperature structure and humidity of the atmosphere. In absence of O₃, the average surface temperature of an Earth-like planet would be 7 K cooler (I. Gomez-Leal et al. 2019). Furthermore, O₃ serves as a filter for incoming UV radiation, safeguarding life on Earth's surface. Therefore, O₃ also plays a role in determining the potential habitability of an exoplanet.

⁵ https://exoplanetarchive.ipac.caltech.edu/docs/counts_detail.html—Date: 15/04/2024.

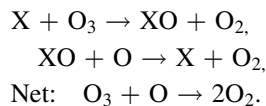
⁶ <https://exoplanets.nasa.gov/what-is-an-exoplanet/planet-types/terrestrial/>—Date: 15/04/2024.



To determine whether an exoplanet harbors life, scientists are keen on detecting biosignatures in its atmosphere. This detection can be achieved through direct imaging or transit spectroscopy. Scientists have considered using O₃ as a proxy to detect molecular oxygen (O₂) in the atmosphere of an exoplanet. However, a study conducted by T. Kozakis et al. (2022) has highlighted that the relationship between O₃ and O₂ is nonlinear and depends on the type of stellar host. This makes it challenging to accurately determine the amount of O₂ through O₃ measurements, especially when the UV flux of the host star is uncertain (G. Cooke et al. 2023). Nonetheless, if we have knowledge about the host star's UV spectrum and certain other information, O₃ measurements might offer insights into the potential habitability of an exoplanet.

On Earth O₃ is primarily produced in the tropical stratosphere via the Chapman mechanism (S. Chapman 1930). During daytime, UV radiation breaks the O₂ molecule to form two O atoms, which then react with O₂ molecules, and a third body M through a three-body process to form O₃. The Brewer–Dobson circulation distributes O₃ in the stratosphere (A. W. Brewer 1949; G. M. B. Dobson 1956; R. E. Newell 1963). In this circulation pattern, air near the tropics rises and then moves toward the poles. The Brewer–Dobson circulation slightly differs between the two hemispheres due to variances in land and ocean structure in the Southern and the Northern Hemispheres (E. E. Remsburg 2015).

This O₃ then either gets photodissociated by UV radiation to form O and O₂, or it reacts with O to form two O₂ molecules. O₃ also gets catalytically destroyed by NO_x, HO_x, Br, and Cl, etc. (R. W. Portmann et al. 2012). If X is a catalytic species, then the O₃ is catalytically destroyed by the following reactions:



In 2016, three Earth-sized planets (TRAPPIST-1b, c, and d) were detected orbiting an ultracool M dwarf star known as TRAPPIST-1 or Two Micron All Sky Survey J23062928-0502285, through observations made by the TRAnsiting Planets and PlanetIsimals Small Telescope (TRAPPIST; M. Gillon et al. 2016). Subsequently, in 2017, Spitzer revealed the existence of four more exoplanets around TRAPPIST-1 (TRAPPIST-1e, f, g, and h), establishing it as the first system with seven Earth-sized planets (M. Gillon et al. 2017). All the planets in the TRAPPIST-1 system are closer to their host star than Mercury is to the Sun.

Future observations with JWST (J. P. Gardner et al. 2006) and new telescopes, such as the Extremely Large Telescope (I. Hook 2009), are expected to reveal more about small rocky exoplanets and their atmospheres. Looking ahead, future concepts like the Habitable Worlds Observatory (National Academies of Sciences, Engineering, & Medicine 2021), which was proposed by combining two earlier concepts—the Habitable Exoplanet Observatory Mission (B. S. Gaudi et al. 2020) and the Large UV/Optical/IR Surveyor (LUVOIR Team 2019)—are anticipated to directly image and characterize the atmospheres of Earth-like exoplanets. Hence, it becomes crucial to model rocky exoplanet atmospheres to aid in interpreting observations by extracting the atmospheric properties and explaining the underlying physical processes occurring in these exoplanetary atmospheres.

In previous studies, general circulation models (GCMs) have been employed to investigate the atmospheres of Earth-like planets, including studies designed to understand the atmospheric circulation and O₃ chemistry of tidally locked Earth-like exoplanets. For example, the TRAPPIST-1 Habitable Atmosphere Intercomparison project (D. E. Sergeev et al. 2022; M. Turbet et al. 2022) compared the results from four GCMs, which included slab oceans for both dry and moist N₂-dominated and CO₂-dominated atmospheres. L. Carone et al. (2018) used the MITgcm to study the stratospheric circulation of a tidally locked exo-Earth scenario for TRAPPIST-1b, TRAPPIST-1d, Proxima Centauri b, and GJ 667 C f. J. S. Yates et al. (2020) employed the Met Office Unified Model to explore the O₃ chemistry of the tidally locked exoplanet Proxima Centauri b around an M dwarf, while E. Proedrou & K. Hocke 2016 used the Community Earth System Model version 1–Whole Atmosphere Community Climate Model (WACCM) model to simulate the 3D O₃ distribution of a tidally locked Earth-like planet around a Sun-like star. A recent study conducted by M. Braam et al. (2023) utilized a slab ocean model of a tidally locked exoplanet around an M dwarf star with Proxima Centauri b parameters to study O₃ spatial distribution. They found that O₃ accumulates on the nightside, demonstrating a dayside–nightside hemispheric asymmetry in O₃ distribution.

Previous studies utilized slab ocean models to study atmospheric circulation on tidally locked exoplanets, resulting in a symmetric atmospheric circulation, as seen in M. Braam et al. (2023). However, many rocky exoplanets may not be completely covered by oceans, and it is unlikely that they will lack ocean dynamics. Furthermore, orography and landmass distribution play a significant role in shaping atmospheric circulation on Earth. In our study we incorporated an Earth-like land–ocean structure to examine for the first time how orography might alter the atmospheric dynamics and chemistry of a tidally locked Earth-like exoplanet modeled on TRAPPIST-1e. Our aim is to characterize the possible O₃ distribution and the influence of atmospheric circulation on it. We focus on O₃ because it is affected by photochemistry, catalytic cycles, and atmospheric transport and has strong spectral features from the UV to the mid-infrared. Additionally, the presence of O₂, a potential biosignature, can be inferred from a detection of O₃.

2. Methods

2.1. Model Description and Setup

For this study, we modeled TRAPPIST-1e using the WACCM version 6 (WACCM6; A. Gettelman et al. 2019). WACCM6 is an atmospheric model that operates as a configuration of the Community Earth System Model version 2 (CESM2). CESM2 is an Earth system model consisting of submodels simulating the atmosphere, ocean, land, sea ice, land ice, river runoff, and surface waves (G. Danabasoglu et al. 2020). The WACCM6 configuration comprises 70 vertical levels, starting from the surface at 1000 hPa and extending up to 140 km at 4.5×10^{-6} hPa (lower thermosphere), with a horizontal resolution of $1^\circ 875$ latitude \times $2^\circ 5$ longitude.

The chemistry applied in WACCM6 is based on the Model of Ozone and Related Chemical Tracers (MOZART). MOZART serves as a global chemical transport model encompassing physical and chemical processes that span the

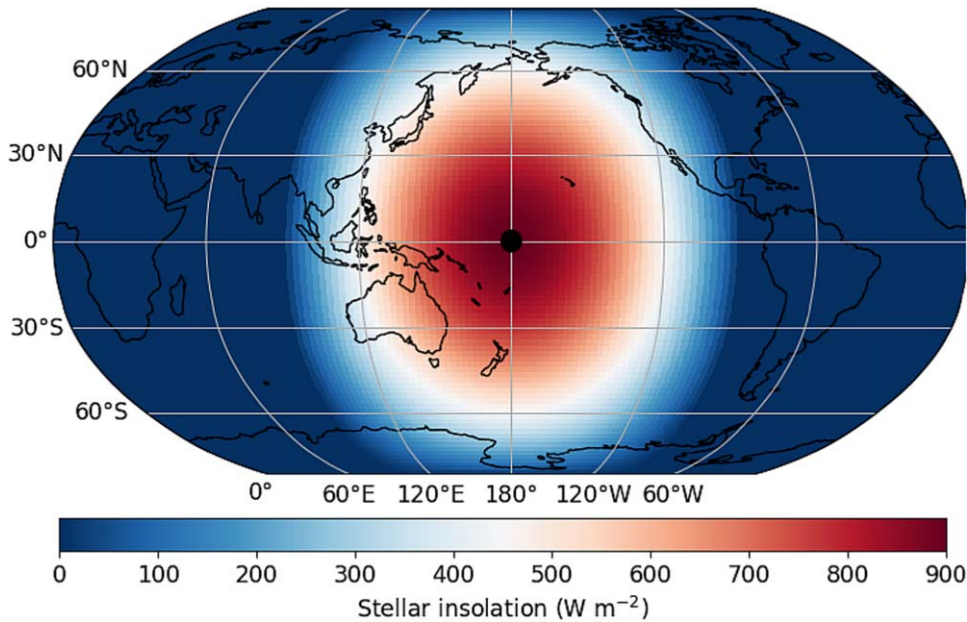


Figure 1. Stellar irradiation received by TRAPPIST-1e in our model. The black dot represents the substellar point, which is fixed at 180° longitude and 0° latitude over the Pacific Ocean. The black outlines represent the land masses.

troposphere, stratosphere, mesosphere, and lower thermosphere (A. J. Conley et al. 2012; L. K. Emmons et al. 2020). WACCM6 employs the Rapid Radiative Transfer Model radiation code for solving longwave (lower energy radiation emitted from the Earth’s surface and atmosphere) and short-wave (higher energy wavelengths such as UV, visible light, and a part of the near-infrared spectrum, associated with the host star) radiative transfer equations. The longwave limit and the shortwave limit used here are $3.08\text{--}1000\ \mu\text{m}$ and $0.2\text{--}12.2\ \mu\text{m}$, respectively.

WACCM6 has been previously utilized to study the climate and O_3 chemistry of prehistoric Earth and Earth-like exoplanets. For example, G. Cooke et al. (2022) demonstrated that the total O_3 column at O_2 concentrations between 0.10% and 50% of the present atmospheric level may have been lower than predicted by previous 1D and 3D models. Possible reasons for this discrepancy include 3D effects and transport, variations in boundary conditions, temperature structure and feedback mechanisms, seasonal cycles, calculations of absorption and scattering within the Schumann–Runge bands, and the condensation of water vapor through the tropical tropopause layer (A. Ji et al. 2023). G. J. Cooke et al. (2023) showed how for an Earth-like exoplanet, observations and spectral signatures of chemical species could be affected by the line of sight, albedo, clouds, and chemistry. B. Liu et al. (2023) studied how changing the eccentricity of an Earth-like exoplanet affects the abundance and loss of water present in the atmosphere.

The model considered here used the BWma1850 compset⁷ of WACCM6, which included a preindustrial Earth-like atmosphere and orography and was modified to allow for synchronous rotation.⁸ The model composition was with O_2 set to present atmospheric level, i.e., 21% by volume and N_2 with 78% by volume. The volume mixing ratios of CH_4 (0.8 ppmv), CO_2 (280 ppmv), N_2O (270 ppbv), and H_2 (500 ppbv) are fixed

Table 1

Planetary Parameters Used for Model of TRAPPIST-1e (Grimm et al. 2018)

Parameter	Units	Value
Semimajor axis	au	0.029
Orbital period	Earth days	6.1
Rotation period	Earth days	6.1
Obliquity	...	0
Eccentricity	...	0
Instellation	W m^{-2}	900
Planet radius	km	5797
Gravity	m s^{-2}	9.14

at the surface. We ran the simulation for 300 yr, of which we utilized the last 40 yr of data in order to eliminate any effects associated with the model adjusting to tidally locked conditions. The substellar point was fixed at 180° longitude and 0° latitude over the Pacific Ocean (see Figure 1). Table 1 shows the parameters used to model TRAPPIST-1e. For this study, we have used a stellar spectrum based on the work of S. Peacock et al. (2019), who modeled the stellar energy distribution of TRAPPIST-1 and produced model 1A, 2A, and 2B, of which we used model 1A, which best matched the TRAPPIST-1 $\text{Ly}\alpha$ reconstruction from V. Bourrier et al. (2017). Figure 2 compares the top-of-the-atmosphere irradiation of TRAPPIST-1e and Earth.

2.2. Data Analysis

For our analysis, we calculated the time average of the 40 yr of data and examined various parameters, including surface temperature, horizontal wind velocities (u and v), vertical wind velocity (w), reaction rates, and volume mixing ratios of O_3 , O_2 , OH , HO_2 , NO , NO_2 , Br , and Cl . To calculate the

⁷ <https://docs.cesm.ucar.edu/models/cesm2/config/2.1.3/compsets.html>

⁸ https://github.com/exo-cesm/CESM2.1.3/tree/main/Tidally_locked_exoplanets/cases

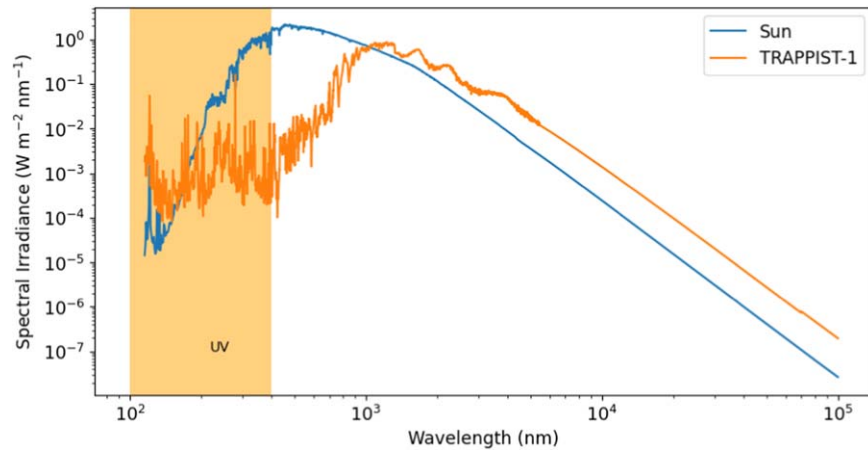


Figure 2. Stellar irradiance at top of the atmosphere of TRAPPIST-1e (orange) and Earth (blue). The orange shaded region represents the range of UV wavelengths.

concentration of chemical species in units of molecules m^{-3} , we multiplied the air number density by the volume mixing ratio of the respective chemical species.

We calculated the O_x production rate using the formula $J_{\text{O}_2} * [\text{O}_2]$, where J_{O_2} is the O_2 photolysis rate constant and $[\text{O}_2]$ is the O_2 concentration. The catalytic destruction rates of O_3 by various chemical species (X) were calculated using the formula $k * [\text{X}] * [\text{O}_3]$, where k is the rate constant for $\text{X} + \text{O}_3$ reactions, $[\text{X}]$ is the concentration of the catalytic species, and $[\text{O}_3]$ is the concentration of O_3 . In this context, X can be OH, HO_2 , NO, NO_2 , Br, or Cl.

To study the horizontal wind circulation, we used the Helmholtz wind decomposition, which has been previously used to study the atmospheric circulations of Earth, tidally locked terrestrial exoplanets, and hot Jupiters (M. Hammond & N. T. Lewis 2021). The Helmholtz wind decomposition breaks down the total horizontal wind into rotational (\mathbf{u}_r) and divergent components (\mathbf{u}_d), allowing us to study the winds responsible for the overall circulation in more detail. For a tidally locked planet, the rotational flow consists of two parts: an equatorial jet (zonal-mean rotational component), which is a narrow belt of winds moving around the equator of a planet, and stationary waves (eddy rotational component). The stationary waves drive the equatorial jet and can accelerate it, resulting in a superrotating jet that moves faster than the planet’s rotation rate (A. P. Showman et al. 2013). The divergent flow consists of a global overturning circulation, which is a result of thermally driven circulation where the air rises on the dayside of the planet and sinks on the nightside. Mathematically, the Helmholtz wind decomposition divides the total circulation given by $\mathbf{u} = (u, v)$ into the two aforementioned components (M. Hammond & N. T. Lewis 2021):

$$\mathbf{u} = \mathbf{u}_d + \mathbf{u}_r = -\nabla\chi + \mathbf{k} \times \nabla\psi, \quad (1)$$

$$\nabla^2\chi = \delta, \quad (2)$$

$$\nabla^2\psi = \zeta. \quad (3)$$

Here, \mathbf{u} represents the horizontal wind vector, where u and v denote the zonal (along latitude) and meridional (along longitude) velocities, respectively. The velocity potential function, χ , is derived from the divergence (δ —Equation (2)), while the streamfunction, ψ , is derived from the vorticity (ζ —Equation (3)) of the wind.

To examine the meridional overturning circulation, we used the meridional mass streamfunction. This is commonly used to

study atmospheric or oceanic circulation patterns and helps in visualizing mass transport in the meridional plane (north–south direction). Mathematically, the relationship between mass streamfunction ψ and both vertical velocity (w) and meridional velocity (v) is expressed by the equation (D. Sidorenko et al. 2020)

$$\frac{1}{R} \frac{\partial\psi}{\partial\theta} = w, \quad \frac{\partial\psi}{\partial z} = -v. \quad (4)$$

Here, θ is the latitude in radians, z is the altitude, and R is the planet’s radius.

3. Results and Discussion

3.1. O_3 Distribution

Figures 3(a) and (b) show the O_3 concentration on the meridional plane passing through the substellar point and the antistellar point for our TRAPPIST-1e model. We consider the profiles at the substellar point and the antistellar point to be representative of the “dayside” and the “nightside,” respectively. O_3 is predominantly present in the lower atmosphere at pressures >10 hPa (below ~ 30 km), and O_3 concentrations are higher near the poles than near the equator. The highest O_3 concentrations are found near the south pole between pressures 600 and 70 hPa (between ~ 5 and ~ 15 km). Further, there is little difference in O_3 concentration between the “dayside” and the “nightside,” much less than the north–south asymmetry, suggesting that the O_3 produced on the dayside gets mixed across longitudes by the horizontal winds.

Figures 4(a) and (b) display the O_3 concentrations at pressures 103 hPa (~ 15 km) and 609 hPa (~ 5 km), respectively. At both of these pressures, the north–south asymmetry in O_3 distribution is clearly visible. It also demonstrates that the difference in O_3 concentration between the dayside and the nightside is significantly smaller compared to the north–south difference (see also Figure 9 (SSPO) in F. Sainsbury-Martinez et al. 2024). On Earth, O_3 produced in the stratosphere near the equator is transported poleward and downward by the Brewer–Dobson circulation, which moves O_3 -rich air toward the poles. This circulation plays a key role in maintaining a relatively symmetric O_3 distribution between the Northern and Southern Hemispheres, though some asymmetries arise due to geographic features, seasonal variations, and polar atmospheric dynamics. The majority of O_3 is located between pressures 300 and 10 hPa. Between pressures 30 and 10 hPa, O_3 is densely

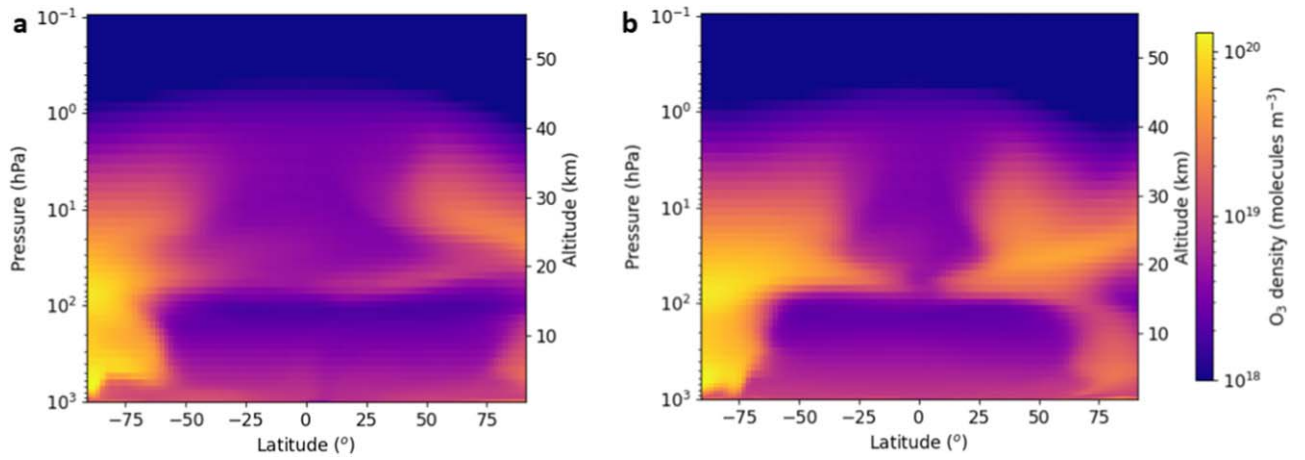


Figure 3. Cross section of the O_3 number density on the meridional plane passing through the (a) substellar point and (b) antistellar point for our TRAPPIST-1e model.

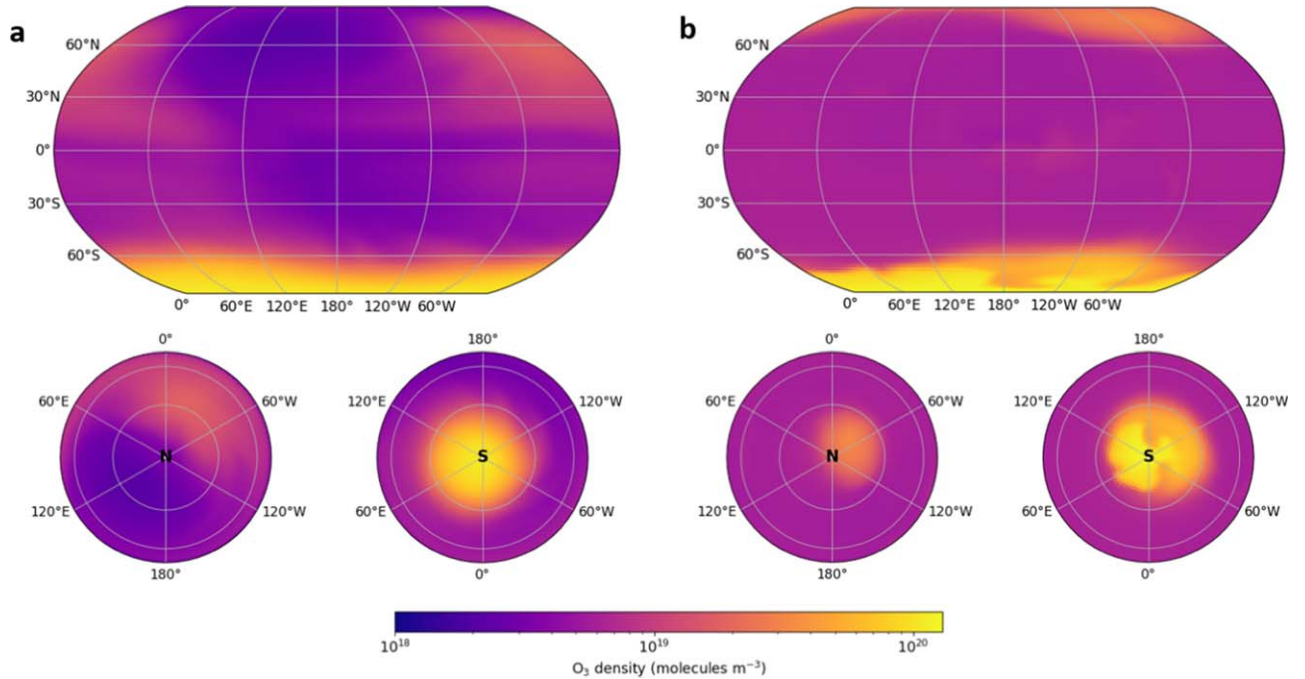


Figure 4. Horizontal slices of the O_3 number density for our TRAPPIST-1e model at a pressure (altitude) of (a) 103 hPa (~ 15 km) and (b) 609 hPa (~ 5 km). The substellar point is at 180° longitude and 0° latitude. N represents the north pole and S represents the south pole. Lower panels show the polar projections.

packed around low latitudes, while between pressures 300 and 30 hPa, O_3 is more abundant around the poles (see L. M. Ejzak et al. 2007). Therefore, the vertical structure and the latitudinal distribution of O_3 in our TRAPPIST-1e model differs significantly from those of Earth.

Figure 5 shows the O_x production rate ($O+O_3$ production rate) on the meridional plane passing through the substellar point. The O_x production rate is symmetric, with peak production occurring in the upper atmosphere (at pressures < 10 hPa or at altitudes above ~ 30 km) due to the large amount of UV radiation received here. UV radiation does not penetrate the lower atmosphere because it becomes denser, absorbing most of the incoming UV radiation, and it is weakest at high latitudes due to geometric effects. Hence, in the lower atmosphere, there is less O_x production near the equator and no production at higher latitudes (as seen in Figure 5, where white areas indicate regions of zero production). When

comparing the pattern of O_3 concentration and O_x production rate, it is evident that the region of peak O_x production rate does not coincide with the region of peak O_3 concentration. There are relatively low O_3 concentrations where the O_x production is high, whereas the region with the highest O_3 concentration (near the south pole between pressures 600 and 70 hPa) has either low or no O_x production. This indicates that O_3 is primarily produced high up in the atmosphere, and either all the O_3 is transported from the upper atmosphere to the lower atmosphere or some of it is transported while the remainder is catalytically destroyed. However, this does not explain the north–south asymmetry in O_3 concentration. To explain this asymmetry, we need to examine if there are asymmetries in catalytic species distribution and atmospheric circulation.

Total O_3 column (TOC) density is reported in Dobson units (DUs), where 1 DU is equivalent to a $10 \mu\text{m}$ thick layer of pure O_3 at 273 K and 1 atm pressure. For Earth the values of TOC

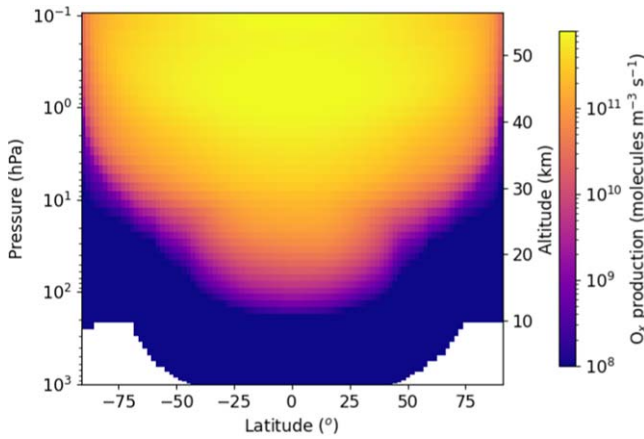


Figure 5. Cross section of O_3 production rate on the meridional plane passing through the substellar point for our TRAPPIST-1e model. The white region on the plot indicates zero production rate.

are 200–250 DU near the South Pole and 300–350 DU near the North Pole.⁹ Figure 6 shows the latitudinal variation in zonal-mean TOC density for both our TRAPPIST-1e model and Earth. From this figure, we clearly observe the north–south asymmetry in O_3 distribution in our TRAPPIST-1e model, whereas O_3 on Earth is roughly symmetrically distributed about the equator. Note that we find that the total O_3 concentration in our TRAPPIST-1e model is much higher compared to that of Earth. The TOC density in our TRAPPIST-1e model near the south pole is 8000 DU, which is around 28 times that of Earth (~ 250 DU), and near the north pole, it is approximately 2000 DU, which is 7 times that of Earth (~ 300 DU). There is slight asymmetry in TOC on Earth with slightly higher TOC near the North Pole as compared to the South Pole, but for our TRAPPIST-1e model, this asymmetry is reversed and significantly larger.

3.2. Role of Catalytic Species

Figure 7 shows the distribution of catalytic species (OH, HO_2 , NO, NO_2 , Cl, and Br) on the meridional plane passing through the substellar point for our TRAPPIST-1e model. For regions at pressures >10 hPa (below ~ 30 km), our initial hypothesis, after observing the symmetric O_x production and the asymmetric distribution of O_3 , was that there might be an uneven distribution of catalytic species. Such an imbalance could potentially be responsible for O_3 depletion being more pronounced near the north pole compared to the south pole. However, our analysis suggests that this is not the case, with the distribution of catalytic species being roughly symmetric and the concentrations low when compared to the O_3 concentration. In the case of Cl (Figure 7(e)) and Br (Figure 7(f)), we find that at pressures >100 hPa the concentrations of these species is slightly higher near the south pole as compared to the north pole; since this is aligned with the peak in O_3 concentration, it cannot explain the high concentrations of O_3 we find at pressures >10 hPa near the south pole.

Figure 8 shows the time taken by the catalytic species to destroy O_3 on the meridional plane passing through the substellar point. We observe that in regions with the highest concentrations of O_3 , catalytic species take longer to destroy O_3

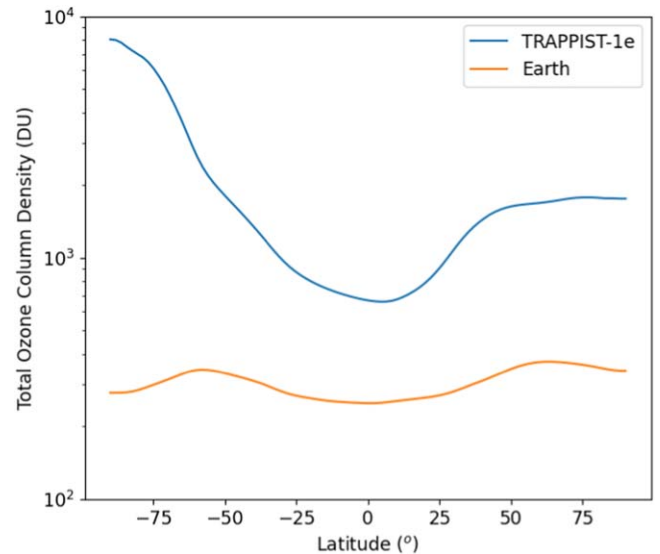


Figure 6. Zonal-mean latitudinal variation of TOC density for our TRAPPIST-1e model (blue) and Earth (orange).

compared to regions where O_3 is produced. The higher concentration of O_3 means there is more O_3 to destroy, and the concentration of catalytic species is low relative to O_3 , leading to a slower overall destruction rate. Furthermore, the replenishment of O_3 through production on the dayside and its transport to the nightside further slows the catalytic destruction process. This observation suggests that at pressures >10 hPa, catalytic destruction occurs at a slower rate, allowing atmospheric circulation to influence the distribution of O_3 . As such, this suggests that catalytic species may not be the primary factor driving the asymmetry in the distribution of O_3 . Therefore, we next look at the transport of O_3 throughout the atmosphere to see if this might have a more significant effect.

3.3. Role of Atmospheric Circulation

Figures 9(a) and (b) show the meridional mass streamfunction on a plane passing through the substellar point and the antistellar point, respectively. We consider the profile at the substellar point to be representative of the “dayside” and the profile at the antistellar point to be representative of the “nightside.” Here, red indicates clockwise transfer of mass and blue indicates counterclockwise transfer of mass. On the “dayside,” without orography we would expect a symmetric circulation with upwelling at the equator, meridional flow toward the poles, downwelling near the poles, and meridional flow from the poles to the equator (see D. E. Sergeev et al. 2022). In our simulation, we find that there is an asymmetry in this circulation: near the north pole the clockwise downwelling is interrupted at 200 hPa and does not reach the surface; rather there is a clockwise meridional transport from the north pole toward midlatitudes, clockwise downwelling at midlatitude, and then clockwise meridional flow from midlatitude toward the equator (Figure 9(a)). The formation of a small counterclockwise (blue) circulation cell near the north pole breaks the symmetry. Similarly, on the “nightside,” without orography we would expect to find upwelling near the poles, meridional transport from the poles to the equator, downwelling at the equator, and meridional transport from the equator toward the poles near the surface, thus closing the global overturning circulation (see D. E. Sergeev et al. 2022). However,

⁹ <https://ozonewatch.gsfc.nasa.gov/SH.html>—Date: 24/08/2023.

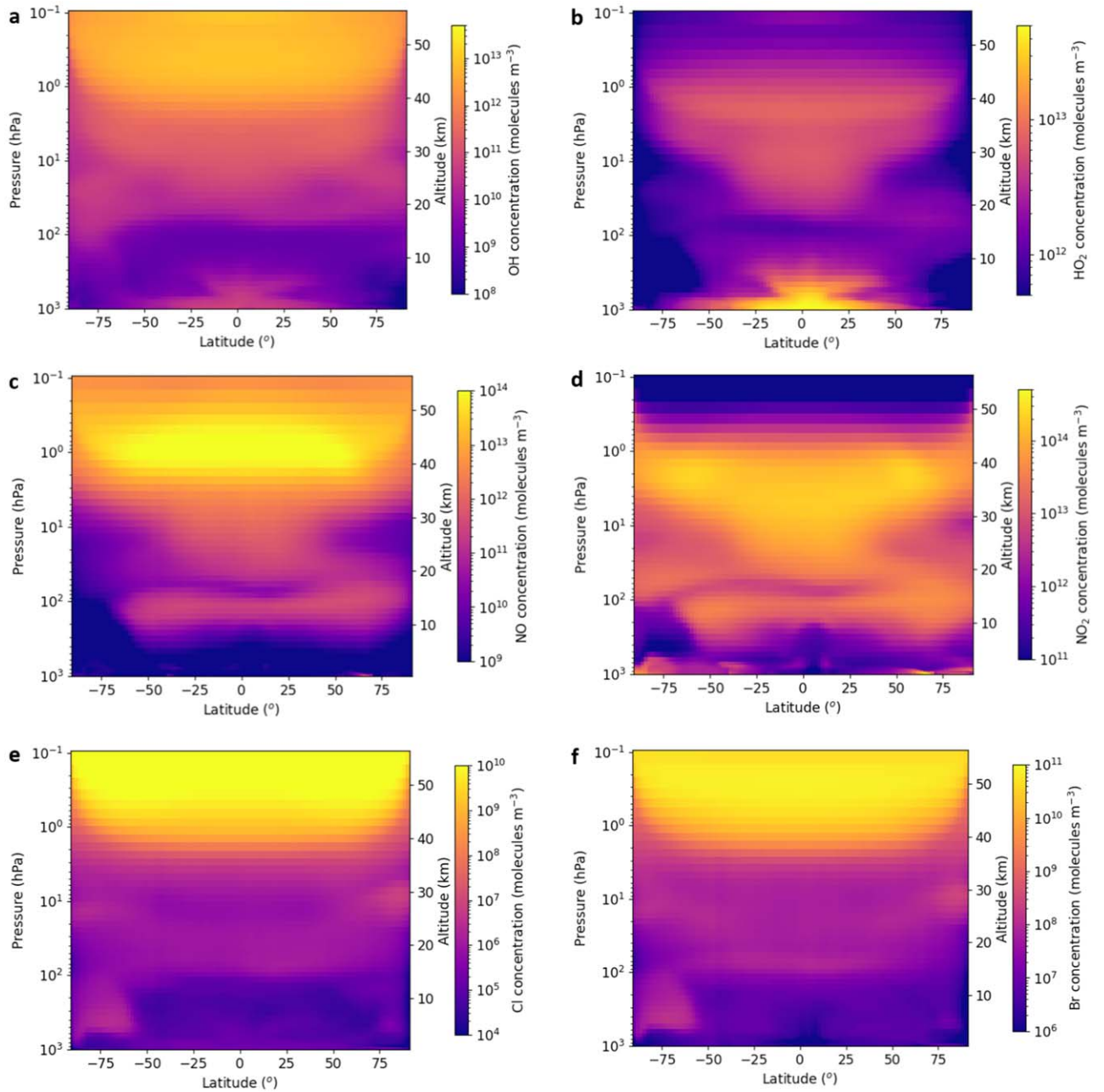


Figure 7. Catalytic species concentration on the meridional plane passing through the substellar point for (a) OH, (b) HO₂, (c) NO, (d) NO₂, (e) Cl, and (f) Br for our TRAPPIST-1e model. The catalytic species are roughly symmetrically distributed, and their concentrations are lower than the O₃ concentrations.

Figure 9(b) reveals there is an asymmetry in this circulation. Near the north pole there are two circulation cells: at pressures <200 hPa, there is counterclockwise upwelling from the north pole, counterclockwise meridional transport from the north pole to the equator, counterclockwise downwelling near the equator until pressure 200 hPa, and counterclockwise meridional transport back to the north pole. At pressures >200 hPa, there is clockwise downwelling near the north pole, clockwise meridional transport from the north pole, across the equator, to the south pole, and then clockwise upwelling near the south pole.

Overall, both on the “dayside” and the “nightside,” we find an asymmetry in the meridional overturning circulation in the northern hemisphere. This asymmetry is caused by the

presence of Earth-like orography. Both on the dayside and the nightside, the northern hemisphere has a higher fraction of landmass compared to the southern hemisphere. This landmass reshapes the winds, leading to the formation of a small counterclockwise cell on the “dayside” and a large clockwise cell on the “nightside,” resulting in an asymmetric meridional overturning circulation in the northern hemisphere.

To visualize the complex horizontal winds, we use Helmholtz wind decomposition, which breaks down the total horizontal wind into its rotational (divergence-free) and divergent (rotation-free) components. Figures 10 and 11 show the divergent component and the eddy rotational component of the horizontal winds in the stratosphere (20 hPa), near the tropopause (103 hPa), and near the surface (800 hPa). When

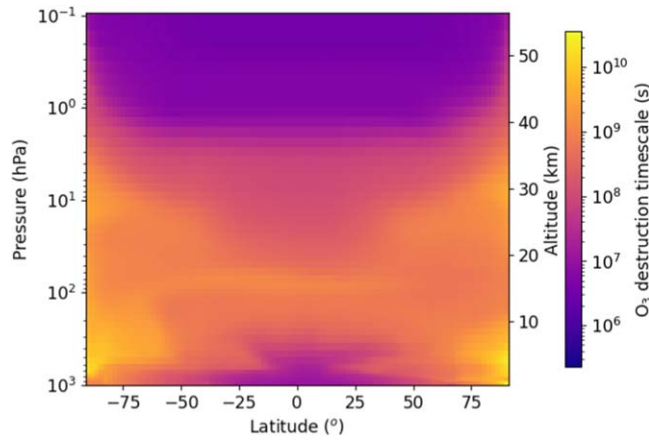


Figure 8. Time taken by the catalytic species to destroy O₃ on the meridional plane passing through the substellar point for our TRAPPIST-1e model.

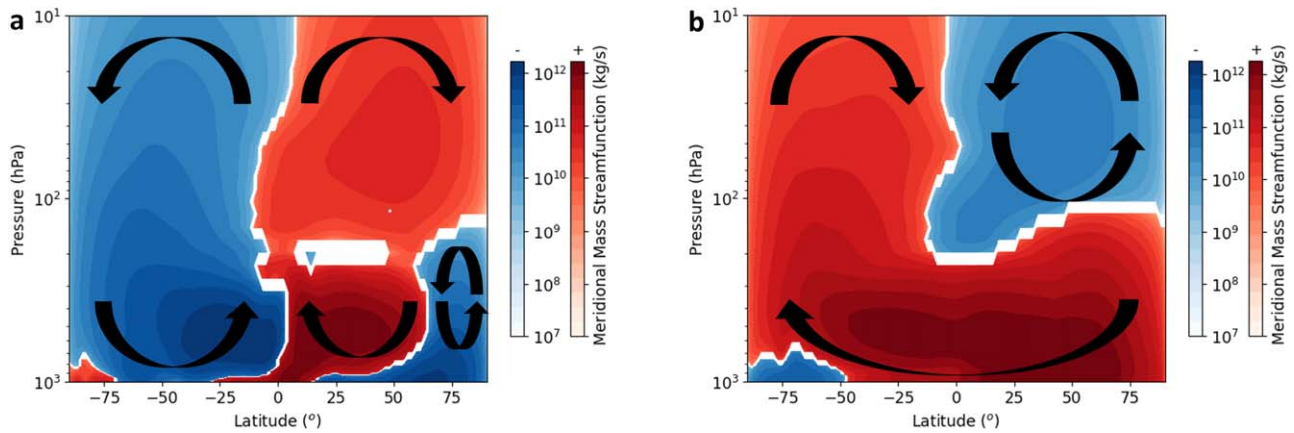


Figure 9. Meridional mass streamfunction on the meridional plane passing through the (a) substellar point and the (b) antistellar point for our TRAPPIST-1e model. The positive values (red) indicate clockwise circulation and the negative values (blue) indicate counterclockwise circulation. The values are in log scale.

comparing the mean wind speeds of both components at each pressure level, we find that the eddy rotational component has a higher mean wind speed than the divergent component. This implies that the eddy rotational component plays a major role in meridional transport.

We can explain the O₃ concentrations' north–south asymmetry using both the meridional overturning circulation and the Helmholtz wind decomposition. O₃ formed on the dayside between pressures 200 and 10 hPa (between ~10 and ~30 km) is evenly transported toward the poles by meridional flow and then from the dayside to the nightside by the rotational component of horizontal winds, which includes both the eddy and zonal-mean components. On the nightside, in the lower atmosphere (at pressures >100 hPa), the meridional flow (see Figure 11(c)) forces large amounts of O₃ from the north pole to the south pole. The north–south asymmetry in the meridional flow, near the surface, on both the “nightside” and the “dayside” occurs due to the presence of Earth-like orography. Land–ocean boundaries and orography significantly influence the near-surface winds, including slowing and redirecting them. For more details, see F. Sainsbury-Martinez et al. (2024). This orographic effect drives a near-surface north-to-south flow on the nightside, disrupting the symmetric day/night transport

found by M. Braam et al. (2023). In our model, most of the surface in the region through which the meridional plane passes through the substellar point is land free, with the exception of the Chukchi Peninsula in the Russian Far East (see Figure 1), which disrupts the near-surface flow in the northern hemisphere, resulting in an asymmetric meridional overturning circulation on the “dayside.” The cells associated with this asymmetry in the northern hemisphere, on both the “dayside” and the “nightside,” prevent O₃ from accumulating near the north pole.

Considering Figures 5 and 11(a) and (b), we find that the O₃ formed at the substellar point between pressures 200 and 10 hPa (between ~10 and ~30 km) is first pushed toward the 120° longitude, then toward the poles, and from the dayside to the nightside by the rotationally driven winds. At pressures >200 hPa (below ~30 km) on the nightside (300°–360° longitude), the flow from the north pole to the south pole (see Figure 11(c)) forces O₃ toward the south pole, which then gets well mixed by the rotational component of the horizontal winds, resulting in high O₃ concentrations in the lower atmosphere near the south pole on both the dayside and the nightside.

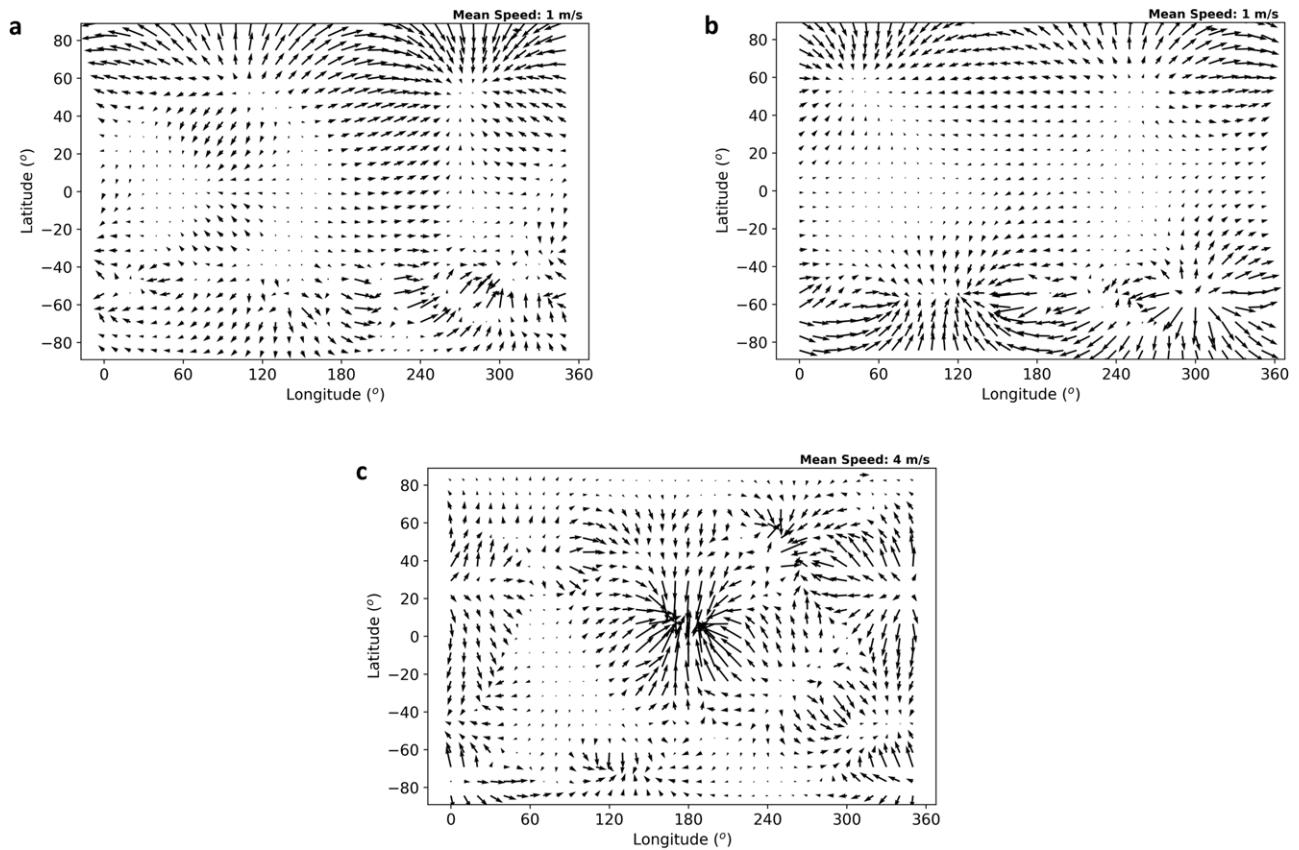


Figure 10. Helmholtz divergent winds at pressures (a) 20, (b) 103, and (c) 800 hPa. Arrows represent wind velocity vectors and point in the direction of flow, with the length of the arrows representing the magnitude of the wind speed (with the mean wind speed shown in the top right corner of each plot).

3.4. Observational Implications

Our results suggest that, for an Earth-like atmospheric composition, TRAPPIST-1e has the potential to exhibit large O_3 concentrations, which could be potentially observable. Furthermore, if O_3 is detected, this would be indicative of atmospheric O_2 . H. Chen et al. (2019) demonstrated through simulated transmission spectra of M dwarf planets that JWST could potentially detect O_3 features during primary transit. However, detecting the prominent O_3 features would require over 100 transits in conditions of zero cloud coverage and twice that number in instances of 100% cloud coverage (J. Lustig-Yaeger et al. 2019). There are numerous factors that influence the O_3 spectral signature, such as the line of sight of the telescope and the presence of other chemical species (E. Proedrou & K. Hocke 2016). The brightness of an exoplanet changes as it orbits its host star and is depicted by the full-phase light curve. This curve shows the entire range of phases from minimum to maximum illumination (S. Seager 2010). The presence of land and ocean masses can lead to nonuniform O_3 distributions as found in our model, and hence, as the planet orbits its host star, the amount of O_3 that is visible might also change. Hence, the detection of O_3 might depend on the phase of the exoplanet we observe. The presence of other chemical constituents in the atmosphere could also hinder O_3 detection by affecting its spectral signature. Chemical constituents that have similar spectral features to O_3 could overlap with O_3 spectral features, making it difficult to detect O_3 . Finally, TRAPPIST-1 is a highly active star with dark spots and bright faculae on its surface, which could make

O_3 detection difficult by interfering with the transmission spectrum of the planet (O. Lim et al. 2023).

3.5. Limitations and Future Work

In this work, we have considered an Earth-like landmass distribution, orography, and atmospheric composition in order to explore the effects of land masses on the atmospheric O_3 distribution, comparing our results to previous studies with slab oceans (M. Braam et al. 2023). In the future, we would like to see studies that expand on our work, while also addressing the Earth-like nature of our assumptions. Suggestions for future work include the following:

1. Our model assumes an Earth-like (N_2 - O_2) atmospheric composition, which is a plausible but uncertain representation of TRAPPIST-1e. The actual atmospheric composition of TRAPPIST-1e remains unknown, and future observations from JWST or other missions could reveal significant differences. For now, our results provide a starting point for exploring potential atmospheric chemistry and dynamics based on an Earth-like scenario. The presence of O_2 is expected to lead to O_3 formation due to UV irradiation, which is a common feature of potentially habitable atmospheres (A. Segura et al. 2003).
2. In our model, 68% of the landmass is situated in the northern hemisphere. Investigating alternative land-ocean distributions—such as an even split, a majority of landmass in the southern hemisphere, or land configurations from different geological periods of

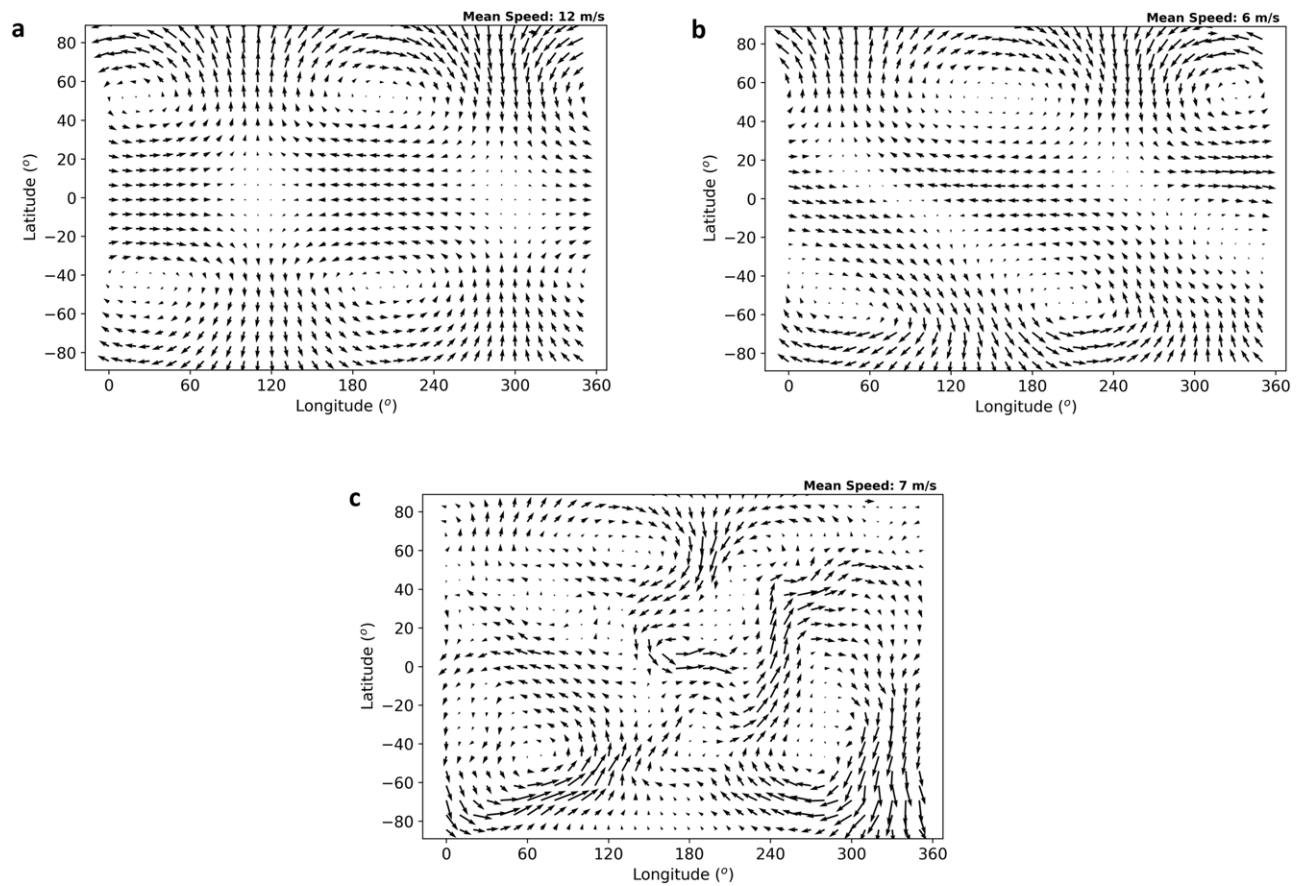


Figure 11. Helmholtz rotational eddy winds at pressures (a) 20, (b) 103, and (c) 800 hPa. Arrows represent wind velocity vectors and point in the direction of flow, with the length of the arrows representing the magnitude of the wind speed (with the mean wind speed shown in the top right corner of each plot).

Earth—could yield valuable insights into how land distribution impacts atmospheric circulation and O_3 accumulation. For example, variations in landmass distribution might influence the poleward transport of O_3 and subsequently affect regional atmospheric dynamics.

3. In our current model, the substellar point is positioned over an ocean, leading to a relatively cold climate on TRAPPIST-1e with limited sources of liquid water. Future investigations should explore the effects of varying land–ocean distribution at the substellar point. This shift in land–ocean configuration could significantly alter the liquid ocean fraction and impact surface evaporation rates. Such changes are expected to influence the atmospheric water vapor content (M. Lague et al. 2023), potentially modifying the distribution of key atmospheric constituents, including O_2 and O_3 .
4. In the future, we could take into consideration the stellar energetic particle flux, resulting NO_x production, and impacts on O_3 . This could potentially lead to a reduction of O_3 at the poles on the nightside. H. Chen et al. (2021) has explored how the atmospheric chemistry on rocky exoplanets is influenced by flares.

4. Summary

In this study, we used the CESM2-WACCM6 GCM to simulate the atmosphere of TRAPPIST-1e, a tidally locked exoplanet, with Earth-like orography and a preindustrial

atmospheric composition, in order to investigate the O_3 distribution and how it is shaped by atmospheric circulations. Our results revealed a significant north–south asymmetry in the O_3 distribution, with concentrations notably higher near the south pole at pressures >10 hPa (below ~ 30 km). The dayside O_x production responsible for O_3 generation is symmetric at lower pressures (higher altitudes) but minimal at higher pressures (lower altitudes), particularly at high latitudes where the insolation is limited. Despite this, we observed a concentrated O_3 abundance near the south pole. This suggested that additional factors, and not just the production of O_x , are shaping the O_3 distribution. One factor we considered, the catalytic destruction of O_3 by species such as OH, HO_2 , NO, NO_2 , Br, and Cl was ruled out due to both the relatively symmetric distribution of said species as well as the low destruction rates.

As such, we turned to the effects of atmospheric circulations on the O_3 distribution. Our analysis revealed an asymmetry in the meridional overturning circulation. This asymmetry is driven by the inclusion of an Earth-like landmass distribution in our model, with land–ocean boundaries shaping near surface winds to drive a flow from the north pole to the south pole on the nightside. On the dayside, the meridional overturning circulation transports O_3 generated at lower pressures (higher altitudes) toward the poles, while the rotational component of the horizontal winds carries O_3 from the dayside to the nightside. On the nightside, the meridional overturning circulation transports O_3 from lower pressures (higher altitudes) to near the surface, where the aforementioned

north-to-south flow carries O₃ toward the south pole. Here, it is then mixed zonally by a wind gyre or vortex. Overall, we find TOC densities up to 28 times higher than Earth at the south pole and 7 times higher than the Earth at the north pole.

Our findings highlight the influence that tidal locking and landmass distribution, including the presence of orography, can exert on the atmospheric circulations and chemical processes of exoplanets, emphasizing the importance of considering these factors, especially land and orography, in future research.

Acknowledgments

We would like to thank the anonymous reviewer for the thorough review and valuable comments that helped us to improve the manuscript. F.S.-M. would like to thank UK Research and Innovation for support under grant No. MR/T040726/1. G.J.C. acknowledges the studentship funded by the Science and Technology Facilities Council of the United Kingdom (STFC; grant No. ST/T506230/1). This work was undertaken on ARC4, part of the High Performance Computing facilities at the University of Leeds, UK.

ORCID iDs

Anand Bhongade  <https://orcid.org/0009-0006-5968-7216>

Daniel R Marsh  <https://orcid.org/0000-0001-6699-494X>

Felix Sainsbury-Martinez  <https://orcid.org/0000-0003-0304-7931>

Gregory Cooke  <https://orcid.org/0000-0001-6067-0979>

References

- Barnes, R. 2017, *CeMDA*, **129**, 509
- Bochanski, J. J., Hawley, S. L., Covey, K. R., et al. 2010, *AJ*, **139**, 2679
- Bourrier, V., Ehrenreich, D., Wheatley, P., et al. 2017, *A&A*, **599**, L3
- Braam, M., Palmer, P., & Decin, L. 2023, in EGU General Assembly 2023 (Vienna: EGU)
- Brewer, A. W. 1949, *QJRMS*, **75**, 351
- Carone, L., Keppens, R., Decin, L., & Henning, T. 2018, *MNRAS*, **473**, 4672
- Chapman, S. 1930, *Mem. Roy. Meteor. Soc.*, **3**, 103
- Chen, H., Wolf, E. T., Zhan, Z., & Horton, D. E. 2019, *ApJ*, **886**, 16
- Chen, H., Zhan, Z., Youngblood, A., et al. 2021, *NatAs*, **5**, 298
- Conley, A. J., Garcia, R., Kinnison, D., et al. 2012, Description of the NCAR Community Atmosphere Model (CAM 5.0) (Boulder, CO: UCAR), https://www2.cesm.ucar.edu/models/cesm1.0/cam/docs/description/cam5_desc.pdf
- Cooke, G., Marsh, D., Walsh, C., Black, B., & Lamarque, J.-F. 2022, *RSOS*, **9**, 211165
- Cooke, G., Marsh, D., Walsh, C., & Youngblood, A. 2023, *ApJ*, **959**, 45
- Cooke, G. J., Marsh, D. R., Walsh, C., Rugheimer, S., & Villanueva, G. L. 2023, *MNRAS*, **518**, 206
- Danabasoglu, G., Lamarque, J.-F., Bacmeister, J., et al. 2020, *JAMES*, **12**, e2019MS001916
- Dobson, G. M. B. 1956, *RSPSA*, **236**, 187
- Dressing, C. D., & Charbonneau, D. 2015, *ApJ*, **807**, 45
- Ejzak, L. M., Melott, A. L., Medvedev, M. V., & Thomas, B. C. 2007, *ApJ*, **654**, 373
- Emmons, L. K., Schwantes, R. H., Orlando, J. J., et al. 2020, *JAMES*, **12**, e2019MS001916
- Gaidos, E., Mann, A. W., Kraus, A. L., & Ireland, M. 2016, *MNRAS*, **457**, 2877
- Gardner, J. P., Mather, J. C., Clampin, M., et al. 2006, *SSRv*, **123**, 485
- Gaudi, B. S., Seager, S., Mennesson, B., et al. 2020, arXiv:2001.06683
- Gettelman, A., Mills, M. J., Kinnison, D. E., et al. 2019, *JGRD*, **124**, 12380
- Gillon, M., Jehin, E., Lederer, S. M., et al. 2016, *Natur*, **533**, 221
- Gillon, M., Triaud, A. H. M. J., Demory, B.-O., et al. 2017, *Natur*, **542**, 456
- Gomez-Leal, I., Kaltenecker, L., Lucarini, V., & Lunkeit, F. 2019, *Icar*, **321**, 608
- Gould, A., Pepper, J., & DePoy, D. L. 2003, *ApJ*, **594**, 533
- Grimm, Demory, B.-O., Gillon, M., et al. 2018, *A&A*, **613**, A68
- Hammond, M., & Lewis, N. T. 2021, *PNAS*, **118**, e2022705118
- Hook, I. 2009, *Science with the VLT in the ELT Era* (Berlin: Springer), 225
- Howard, A. W., Marcy, G. W., Bryson, S. T., et al. 2012, *ApJS*, **201**, 15
- Huang, S.-S. 1959, *PASP*, **71**, 421
- Ji, A., Kasting, J. F., Cooke, G. J., Marsh, D. R., & Tsigaridis, K. 2023, *RSOS*, **10**, 230056
- Kozakis, T., Mendonca, J. M., & Buchhave, L. A. 2022, *A&A*, **665**, A156
- Lague, M., Quetin, G., Ragen, S., & Boos, W. 2023, *CIDy*, **61**, 5309
- Lim, O., Benneke, B., Doyon, R., et al. 2023, *ApJL*, **955**, L22
- Liu, B., Marsh, D. R., Walsh, C., & Cooke, G. 2023, *MNRAS*, **524**, 1491
- Lustig-Yaeger, J., Meadows, V. S., & Lincowski, A. P. 2019, *AJ*, **158**, 27
- LUVOIR Team 2019, arXiv:1912.06219
- Mulders, G. D., Pascucci, I., & Apai, D. 2015, *ApJ*, **814**, 130
- National Academies of Sciences, Engineering, and Medicine 2021, *Decadal Survey on Astronomy and Astrophysics 2020* (Washington, DC: National Academies Press)
- Newell, R. E. 1963, *QJRMS*, **89**, 167
- Nutzman, P., & Charbonneau, D. 2008, *PASP*, **120**, 317
- Peacock, S., Barman, T., Shkolnik, E. L., Hauschildt, P. H., & Baron, E. 2019, *ApJ*, **871**, 235
- Portmann, R. W., Daniel, J. S., & Ravishankara, A. R. 2012, *RSPTB*, **367**, 1256
- Proedrou, E., & Hocke, K. 2016, *EP&S*, **68**, 96
- Reiners, A., Zechmeister, M., Caballero, J., et al. 2018, *A&A*, **612**, A49
- Remsberg, E. E. 2015, *ACP*, **15**, 3739
- Sainsbury-Martinez, F., Walsh, C., Cooke, G. J., & Marsh, D. R. 2024, *ApJ*, **974**, 139
- Seager, S. 2010, *Exoplanets* (Tucson, AZ: Univ. of Arizona Press)
- Segura, A., Krellove, K., Kasting, J. F., et al. 2003, *AsBio*, **3**, 689
- Sergeev, D. E., Fauchez, T. J., Turbet, M., et al. 2022, *PSJ*, **3**, 212
- Shields, A. L., Ballard, S., & Johnson, J. A. 2016, *PhR*, **663**, 1
- Showman, A. P., Wordsworth, R. D., Merlis, T. M., & Kaspi, Y. 2013, in *Comparative Climatology of Terrestrial Planets*, ed. S. J. Mackwell et al. (Tucson, AZ: Univ. of Arizona Press), 277
- Sidorenko, D., Danilov, S., Koldunov, N., Scholz, P., & Wang, Q. 2020, *GMD*, **13**, 3337
- Turbet, M., Fauchez, T. J., Sergeev, D. E., et al. 2022, *PSJ*, **3**, 211
- Yates, J. S., Palmer, P. I., Manners, J., et al. 2020, *MNRAS*, **492**, 1691